Quantum Electronics **50** (4) 335–342 (2020)

https://doi.org/10.1070/QEL17263

Generation of gamma radiation by a subterawatt ultrashort laser pulse: optimisation of preplasma and pulse duration

S.A. Shulyapov, I.N. Tsymbalov, K.A. Ivanov, G.A. Gospodinov, R.V. Volkov, V.Yu. Bychenkov, A.B. Savel'ev

Abstract. **We report an experimental and numerical study of the acceleration of electrons in a plasma interacting with a subterawatt laser pulse (intensity of $\sim 3 \times 10^{18}$ W cm^{-2} at a pulse duration of 50 fs). A preplasma layer on the surface of a molybdenum target is formed by an additional laser pulse with a duration of 8 ns and an intensity of $\sim 2 \times 10^{12}$ W cm^{-2}. It is shown that an increase in the laser pulse duration to 1700 fs at a constant energy (and a proportional decrease in intensity) leads to an increase in the yield of bremsstrahlung γ-radiation by more than an order of magnitude when the nanosecond pulse is ahead of the femtosecond one by 15–25 ns. Interferometry data and results of diagnostics of optical and γ-radiation of a plasma demonstrate that the collisional ionisation of atoms by electrons oscillating in the field of such a laser pulse plays an essential role in the formation of electron density profile. The sensitivity of the described effect to the level of amplified spontaneous emission is determined, despite the nanosecond pulse impact. Numerical simulations show that at a large pulse duration, the acceleration of electrons is stipulated by the beaking of plasma waves excited during stimulated Raman scattering of laser radiation.**

Keywords: *subrelativistic intensity, preplasma, contrast, amplified spontaneous emission, laser plasma, electron acceleration, collisional ionisation.*

1. Introduction

Femtosecond (FS) laser plasma is a bright source of high-energy electrons which, when propagating in a substance, lead to the generation of hard bremsstrahlung X- and gamma rays [1–3]. Prepulses or amplified spontaneous emission (ASE) accompanying the main laser pulse can form a plasma layer on the target surface, which largely determines the electron acceleration mechanisms. Processes occurring in plasma at different contrasts, radiation intensities, and pulse durations are widely discussed in the literature [4–7]. However, the issue of their optimisation to increase the generation efficiency of fast relativistic electrons remains unresolved.

Ivanov et al. [8] showed that at a low ASE level contrast of the pulse (10^{-5}), an increase in its duration from 45 to 350 fs at the same energy (with an intensity decreased from 7×10^{17} to 9×10^{16} W cm^{-2}) leads to a significant increase in the yield and energies of γ-quanta generated in the interaction of radiation with metal targets (steel, lead). At the same time, with a high ASE level contrast of the pulse (10^{-8} in [8]), the described effect was not observed [7, 9].

In order to study plasma processes by controllably changing preplasma layer parameters, Shulyapov et al. [10] and Ivanov et al. [11] used a nanosecond (NS) pulse (~10 ns) as an artificial prepulse for the main FS pulse of relativistic intensity (50 fs, 3×10^{18} W cm^{-2}) with good contrast (10^{-7}). In the scheme with an artificial NS prepulse, an increase in the maximum energy of γ-radiation by more than 7 times was observed in comparison with the case of a single FS pulse [11]. A collimated high-energy electron beam with a large charge [divergence of ~50 mrad, temperature (spectrum slope) of ~2 MeV, charge of ~10 pC] was recorded using the same scheme [12].

This paper presents the results of studies on the generation of γ-radiation in the presence of an artificial NS prepulse at various FS pulse durations. It is shown that an increase in the FS pulse duration from 50 to 1700 fs, when the NS prepulse is ahead of the main pulse by about 20 ns, leads to an increase in the γ-radiation yield from plasma by more than 10 times. In this case, the energies of the generated γ-quanta significantly exceed the oscillatory energies of electrons (~10–30 keV), corresponding to the intensities of chirped FS pulses. Numerical simulation has shown that acceleration of electrons is stipulated by the development of parametric processes in plasma, and the required plasma gradient is formed due to collisional ionisation by electrons oscillating in the FS pulse field.

2. Experimental setup

A scheme of the experimental setup is shown in Fig. 1. A Ti:sapphire laser with a centre wavelength of $\lambda_0 = 813$ nm and a pulse repetition rate of 10 Hz was used to generate the p-polarised radiation. With a minimum FS pulse duration

S.A. Shulyapov, G.A. Gospodinov, R.V. Volkov Faculty of Physics, Lomonosov Moscow State University, Vorob'evy gory, 119991 Moscow, Russia; e-mail: ser270489@yandex.ru;
I.N. Tsymbalov International Laser Centre, Lomonosov Moscow State University, Vorob'evy gory, 119991 Moscow, Russia; Institute for Nuclear Research, Russian Academy of Sciences, prosp. 60-letiya Oktyabrya 7a, stroenie 3, 117312 Moscow, Russia;
K.A. Ivanov, A.B.Savel'ev Faculty of Physics, Lomonosov Moscow State University, Vorob'evy gory, 119991 Moscow, Russia; Lebedev Physical Institute, Russian Academy of Sciences, Leninsky prosp. 53, 119991 Moscow, Russia;
V.Yu. Bychenkov Lebedev Physical Institute, Russian Academy of Sciences, Leninsky prosp. 53, 119991 Moscow, Russia

Received 6 February 2020; revision received 4 March 2020
Kvantovaya Elektronika **50** (4) 335–342 (2020)
Translated by M.A. Monastyrskiy

(FWHM) $\tau_0 = 50 \pm 5$ fs and an energy of 25 mJ, the maximum radiation intensity I_0 on the target reaches $\sim 3 \times 10^{18}$ W cm^{-2} (an integral energy flux density $F_0 \approx 1.5 \times 10^5$ J cm^{-2}). The pulse duration was increased to 1700 fs by changing the distance between diffraction gratings in a laser system compressor.

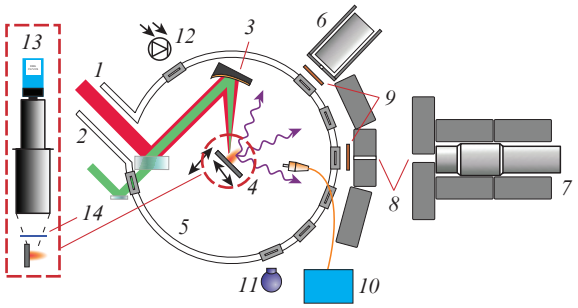

Figure 1. Experimental setup:
(*1*) Ti:sapphire laser radiation; (*2*) Nd:YAG laser radiation; (*3*) parabolic mirror; (*4*) target; (*5*) vacuum chamber; (*6*, *7*) scintillation detectors; (*8*) collimators; (*9*) metallic (Pb, W, Cu) filters; (*10*) optical spectrometer; (*11*) video camera; (*12*) photodiode; (*13*) microscope with a camera located above the target (optical axis is perpendicular to the plane of incidence of radiation on the target); (*14*) interference filter.

The third-order autocorrelation function of the FS pulse is shown in Fig. 2. The temporal profile of the FS pulse contains prepulses with a delay of –20 ps and –14 ns at a contrast of $\sim 4 \times 10^{-5}$ and $\sim 5 \times 10^{-8}$, respectively (when the delay is negative, the NS pulse is ahead of the FS pulse); the ASE level contrast is $\sim 10^{-7}$ for delays from –50 to –175 ps. The contrast can be increased by using a scheme based on the generation of a cross-polarised wave (XPW) in the laser system [13], with the ASE level falling below 10^{-9}.

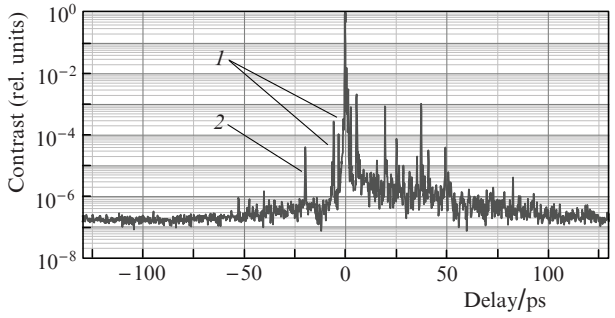

Figure 2. Third-order autocorrelation function of the FS pulse (without using the XPW scheme): (*1*) artefacts; (*2*) prepulse with a delay of –20 ps.

To generate an artificial NS prepulse, we used a *Q*-switched Nd:YAG laser. The radiation wavelength was 1064 nm at a pulse duration (FWHM) of 8 ns, an energy of 150 mJ, and a target intensity of $\sim 2 \times 10^{12}$ W cm^{-2}. The delay between the maxima of the FS and NS pulses was set from –50 to 10 ns with an accuracy of ~1 ns, which was controlled by EOT's ET-2000 photodetector.

The FS and NS radiation beams were superimposed in space using a dichroic mirror mounted in front of an off-axis parabolic (OAP) mirror (a focal length of 76.2 mm with *f*/5 and *f*/8 for FS and NS radiations, respectively), which focused both beams onto the target at an angle of 45° to the normal. To measure the size of the beams and to control their concentricity, the image of the OAP focal plane was transmitted with a magnification to the CCD camera array using a micro objective (numerical aperture NA = 0.3) installed instead of the target. The beam diameters (FWHM) were ~2.5 and ~15 μm for FS and NS radiations, respectively. Since the Rayleigh length for the NS beam (~150 μm) was significantly greater than that for the FS beam (~10 μm), the target displacement along the beam axis allowed the position of the FS pulse focusing point to be controlled above the target surface without significantly affecting the plasma gradient generated by the NS pulse.

As a target, we used 2-mm-thick molybdenum (Mo) plates mounted on a three-axis translation stage, which made it possible to move the interaction region onto the intact target surface after each laser pulse, as well as to shift the target plane along the focal axis. Laser-plasma interaction occurred in a vacuum chamber at a residual gas pressure of $\sim 10^{-2}$ Torr.

Gamma radiation was recorded using NaI (Tl) crystal-based scintillation detectors shielded with lead blocks and closed from plasma by metal filters. One of the detectors (with a 70-mm-thick crystal) measured the integral intensity of γ-radiation. Additional diaphragms attenuating the γ-radiation flux were placed in front of the second detector (63-mm-thick crystal), which made it possible to transfer the γ-radiation flux to a single-quantum regime for measuring the γ-radiation spectra that allowed the temperature of fast plasma electrons to be evaluated [8, 14]. By temperature we mean a parameter T that determines the decay steepness of the energy spectrum $N(E)$ of electrons or γ-quanta, provided that the spectrum is approximated by the function $\exp(-E/T)$.

The spectra of optical plasma radiation were measured with a Solar S150-II spectrometer, the receiving fibre of which was located close to the axis of the laser beam reflected from the target. The spectrum and directivity of the optical radiation of plasma were also monitored by a video camera.

Optical radiation sources were visualised by imaging the laser-plasma interaction region to the camera array (Imaging source DMK 33GV024 camera) using a microscope located above the target. The optical axis of the microscope was perpendicular to the plane of incidence of laser radiation onto the target. Interference filters were installed in front of the microscope lens to allow radiation to pass through certain wavelength ranges. For example, a Thorlabs FB550-40 filter transmitting radiation with $\lambda = 550 \pm 40$ nm was used to record the three-halves harmonic of the FS pulse.

The electron density gradient was restored on the basis of an interference pattern formed by a part of the probe beam passing through a plasma torch and by a part of the same beam propagating in vacuum. For restoration, we used the phase incursion obtained in plasma and applied the inverse Abel transform. The electron gradient was considered to be symmetrical relative to the axis of the laser beam forming the plasma. The technique of conducting the experiment and processing the results is described in [15]. The interference pattern was analysed for the minimum duration of the FS pulse. The plasma torch was formed by a combination of NS and FS pulses (an intensity of $\sim 10^{18}$ W cm^{-2}). A scanning pulse with a wavelength of 406 nm and a duration of 50 fs followed the FS pulse with a delay of 1 ps. Scanning was performed paral-

lel to the target surface in the plane of incidence of the FS and NS beams.

3. Diagnostics of laser plasma

Figure 3 shows the dependences of the integral yield N_γ of γ-radiation from plasma on the delay time Δt_0 between NS and FS pulses and the position f_0 of the focusing point of the FS beam relative to the original target surface (gamma radiation maps) when the point centres of the NS and FS beams on the target exactly coincide. In this case, $f_0 > 0$ corresponds to a scenario when the FS beam is focused above the target surface, and $\Delta t_0 < 0$ corresponds to a scenario when the NS pulse maximum is ahead of the FS pulse. Measurements were performed for the FS pulse durations $\tau \approx 50$, 600, 1150, and 1700 fs, which corresponded to the intensities $I \approx 3 \times 10^{18}$, 2×10^{17}, 1×10^{17} and 8×10^{16} W cm^{-2}, since the FS pulse energy did not change. The detector was covered with a 4-mm-thick lead filter and recorded γ-quanta with energies exceeding 250 keV. Each point of the map was obtained as a result of averaging over approximately 30 laser pulses.

At a minimum duration of the FS pulse (Fig. 3a), there are two regions with an increased γ-radiation yield: for small delays Δt_0(from +5 to –10 ns) and for large delays $\Delta t_0 <$ –20 ns (hereinafter, the first and the second maxima), as well as the range of delays with Δt_0 from –10 to –20 ns, in which γ-radiation virtually disappears (hereinafter, a dip). The presence of regions of the first maximum and a dip at a minimum duration of the FS pulse was discussed earlier in our work [11]. When the FS pulse duration increases (Figs 3b–3d), the integral yield of γ-radiation (with an energy exceeding 250 keV) increases at the second maximum by more than 10 times compared to original level, by 2–3 times compared to the yield at the first maximum with a minimum duration, and by 30 times compared to the yield in the case of a single FS pulse without a NS prepulse. In this case, the second maximum is shifted to the region $f_0 > 100$ μm, i.e., this region is located above the target surface. At the same time, the first maximum significantly weakens and the dip region also becomes less pronounced. We should note that the observed effect of increasing the γ-radiation yield does not depend on chirp sign of the FS pulse.

The γ-radiation spectra were measured by focusing the FS pulse near the target surface ($f_0 \approx 0$) in the first maximum region ($\Delta t_0 = 0$) at a minimum pulse duration, as well as in the second maximum region ($\Delta t_0 = -20$ ns) at a pulse duration increased to 1130 ± 70 fs. The temperatures of fast electrons for the obtained spectra did not differ significantly and amounted to 400 ± 50 keV, whereas in the case of a single FS pulse without a NS prepulse they amounted to 180 ± 20 keV.

Despite the fact that the NS prepulse plays a crucial role in the interaction regime in question, the ASE level contrast of the FS pulse is also a critical parameter. In particular, when the contrast increases from 10^{-7} to 10^{-9} according to the XPW scheme, the second maximum disappears completely, along with the effects associated with an increase in the FS pulse duration. In this case, when using the NS pulse, the effect of increasing the quantum energy and the γ-radiation yield at the first maximum is preserved. In general, the ASE level significantly affects the yield and energy of γ-radiation quanta. However, in the framework of this work, we limit ourselves to describing effects at a fixed ASE level of $\sim 10^{-7}$.

An increase in the FS pulse duration is accompanied by a significant change in the optical radiation spectrum of plasma in the second maximum region (Fig. 4a). In the case of a minimum pulse duration, the fundamental harmonic spectrum of FS radiation (ω_0) is significantly broadened into the blue region due to changes in the plasma refractive index during ionisation by the FS pulse [16]. The spectrum width $\Delta\omega_i$ reaches ~150 nm. As the FS pulse duration increases, the ionisation broadening decreases. Spectral components appear near 530 nm, being close in wavelength to the three-halves harmonic ($3\omega_0/2$) of the FS pulse. This harmonic is a characteristic feature of the development of parametric processes in plasma in the vicinity of $n_e \approx n_{cr}/4$, where n_e is the electron density and $n_{cr} = 1.74 \times 10^{21}$ cm^{-3} is the critical electron density for $\lambda_0 = 0.8$ μm [17, 18]. The wavelength shift of the three-halves harmonic to the blue (by about 10 nm) may be associ-

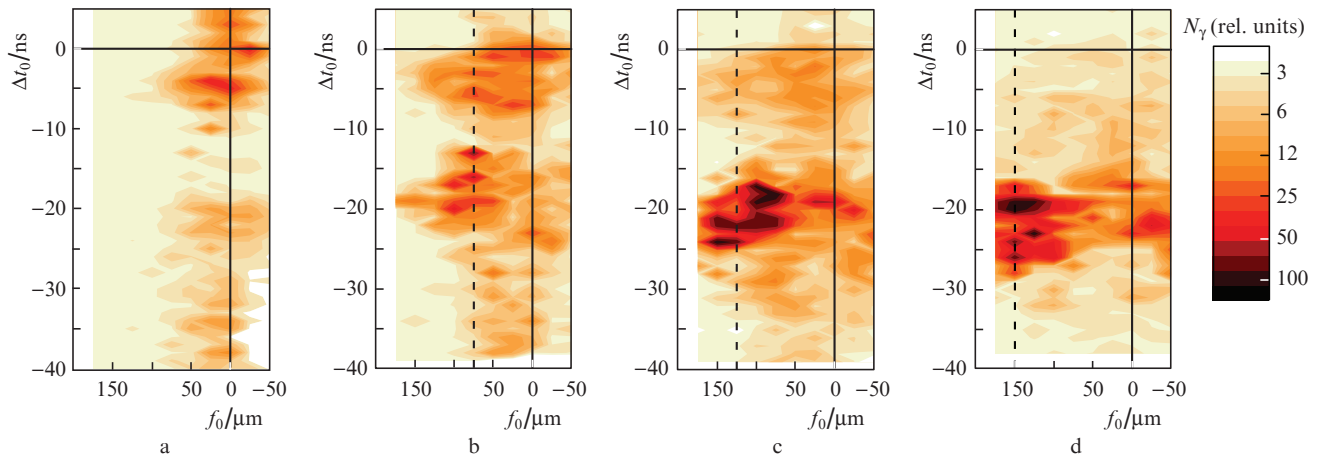

Figure 3. (Colour online) Maps of the integral yield of γ-radiation from N_γ plasma for different durations τ of the FS pulse and constants of its energy: (a) $\tau = 50 \pm 5$ fs and $I \approx 3 \times 10^{18}$ W cm^{-2}, (b) $\tau = 570 \pm 40$ fs and $I \approx 2 \times 10^{17}$ W cm^{-2}, (c) $\tau = 1130 \pm 70$ fs and $I \approx 1 \times 10^{17}$ W cm^{-2}, and (d) $\tau = 1700 \pm 100$ fs and $I \approx 8 \times 10^{16}$ W cm^{-2}. Solid lines correspond to $f_0 = 0$ and $\Delta t_0 = 0$, dashed lines indicate the position of the FS pulse focus at which N_γ is maximum.

ated with ionisation broadening of the fundamental harmonic.

Figure 4b shows images of the laser-plasma interaction region obtained using a microscope with a filter that transmits radiation at the wavelength of the three-halves harmonic (550 ± 40 nm). In the second maximum region, the three-halves harmonic source is located above the target surface, and the distance from it to the target surface depends on the FS pulse duration. As its duration increases, the source shifts away from the target surface, similar to the optimal focusing point for generating γ-radiation (see Fig. 3). In this case, the source position is almost independent of the focusing point of the FS pulse. The brightest three-halves harmonic appears when the FS pulse is focused into the region where the harmonic source is located (the γ-radiation yield is also maximum), and disappears when the focusing point of the FS pulse is significantly shifted (~50–100 μm).

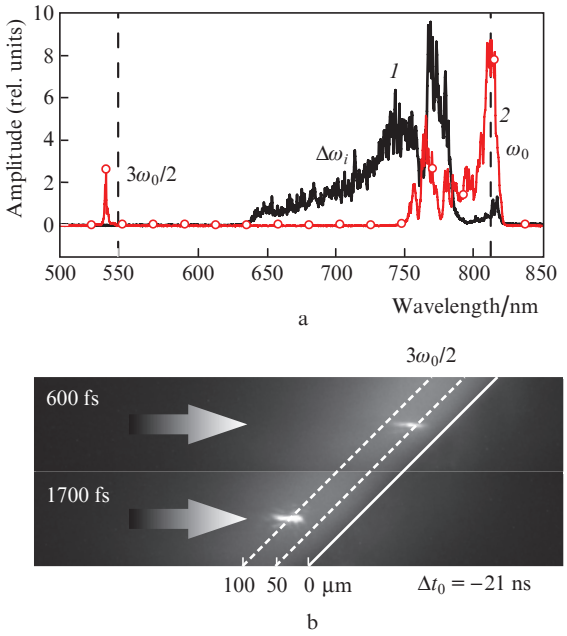

Figure 4. (a) Optical plasma radiation spectra in the second maximum region ($\Delta t_0 = -23$ ns, $f_0 = 75$ μm) for the FS pulse duration of (*1*) 50 and (*2*) 600 fs; dashed lines indicate the centre wavelength of FS radiation (813 nm) and the calculated position of its three-halves harmonic (542 nm); (b) images obtained using a microscope show the location of a source of the three-halves harmonic ($3\omega_0/2$) in the second maximum region ($\Delta t_0 = -21$ ns) with a pulse duration of (top) 600 fs and (bottom) 1700 fs; the solid line corresponds to the target surface position, and dashed lines are displaced by 50 and 100 μm above the target surface.

Figure 5 presents typical shadow photographs of plasma generated only by an NS pulse and a combination of NS and FS pulses, along with the density profile of plasma electrons for the latter case, obtained by optical interferometry. The delay between NS and FS pulses was –30 ns, i.e., it corresponded to the second maximum region. The main FS pulse (a duration of 50 fs, a radiation intensity of $\sim 10^{18}$ W cm^{-2}, and an integral energy flux density $F \sim 0.5 \times 10^5$ J cm^{-2}) was focused onto the target surface ($f_0 = 0$). In the plasma shadow region in the presence

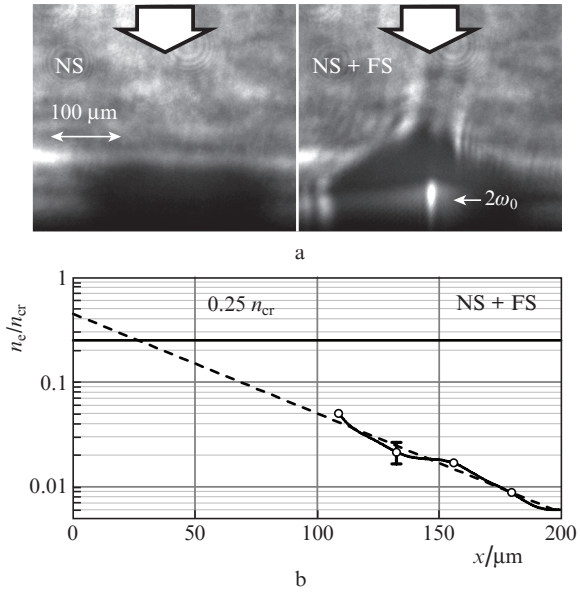

Figure 5. (a) Shadow photographs of a plasma cloud formed by (left) a NS pulse only and (right) a combination of NS and FS pulses; the lower boundary of the image corresponds to the target surface, and the arrow shows the directions of the laser pulse propagation. (b) The electron density profile on the beam axis (solid curve) and its extrapolation ($n_e = A\exp(-x/x_0)$) to the region of smaller x from the target surface (dashed line), obtained when the NS and FS pulses are combined.

of the FS pulse (see Fig. 5a), the plasma radiation source is visible at the frequency of the second optical harmonic ($2\omega_0$) of the FS radiation.

With large delays between the NS and FS pulses (in the Δt_0 range from –20 to –30 ns), against the background of the plasma cloud formed by the NS pulse, the plasma generated under the FS pulse action begins to make a more significant contribution to the electron density distribution. In the absence of the FS pulse, the n_e profile is noticeably narrowed, which is clearly visible even in shadow photographs (see Fig. 5a). At the same time, the electron density n_e is significantly less than the value of $0.25\,n_{cr}$ corresponding to effective parametric excitation of plasma waves (see Fig. 5b). The key factor determining the appearance of the plasma gradient is the impact of ASE, the intensity of which at a contrast of $\sim 10^{-7}$ exceeds 10^{11} W cm^{-2}. The electron density can also increase due to the field and collisional ionisation in the FS pulse field.

4. Discussion of experimental results and the role of collisional ionisation

A decrease in the ionisation broadening $\Delta\omega_i \propto (dn_e/dt)L$ with an increase in the FS pulse duration indicates a decrease in the ionisation rate dn_e/dt, since the preplasma gradient is formed by the action of the NS pulse and the ASE pedestal of the main FS pulse, while the length L where the electron density is nonzero does not change. The coincidence of the focusing regions of the FS pulse, at which the yields of γ-radiation and three-halves optical harmonic are maximum, indicates the necessity of exciting plasma waves for effective electron acceleration. On the other hand, the generation of the three-halves harmonic above the target surface (see

Fig. 4b) is only possible at the electron density $n_e \approx n_{cr}/4$ in this region. However, interferometry data (see Fig. 5b) show that at a distance of 75–150 μm above the target surface, the electron density is significantly less.

With an increase in the FS pulse duration and a shift of its focusing point, the electron density may increase due to ionisation in the FS pulse field (field and collisional ionisation). Let us estimate an increase in the electron density n_e under conditions of an experiment with an increased FS pulse duration (in comparison with the interferometry data) when only field ionisation is taken into account. Using the FS pulse parameters and the Landau formula for the probability of field ionisation [19–21], we can estimate the dependence of the field ionisation multiplicity $Z_f(x)$ of the target atoms at the beam axis on the distance x to its surface.

Figure 6 presents the ratio of $\chi(x) = Z_f(x, \tau, f_0, F_0)/Z_f(x, 50\text{ fs}, 0\ \mu\text{m}, 0.5 \times 10^5\ \text{J cm}^{-2})$, i.e., the ionisation multiplicity by focusing long (τ = 600, 1150 and 1700 fs) FS pulses with an integral energy flux density of $F_0 \approx 1.5 \times 10^5$ J cm^{-2} in the corresponding regions where an increased yield of γ-radiation was observed (f_0 = 75, 125 and 150 μm, see Fig. 3), to the ionisation multiplicity under conditions corresponding to Fig. 5b. With allowance for the relation $n_e = n_a Z_f$, where n_a is the density of atoms, the evaluation shows that the electron density in the regions under consideration increases no more than twice as compared to the interferometry results.

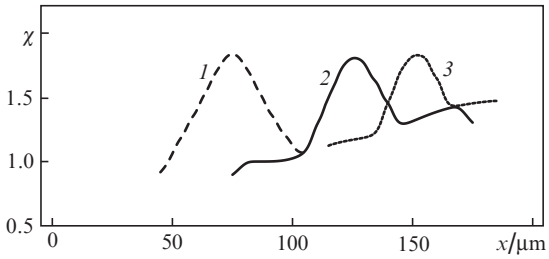

Figure 6. Ratio χ of the field ionisation multiplicity Z_f for Mo atoms on the axis of FS radiation with an integral energy flux density of $F_0 \approx 1.5 \times 10^5$ J cm^{-2} and a duration of τ = 600 fs, being focused at point f_0 = 75 μm above the target surface (*1*), τ = 1150 fs, f_0 = 125 μm (*2*) and τ = 1700 fs, f_0 = 150 μm (*3*), to the ionisation multiplicity at $F \approx 0.5 \times 10^5$ J cm^{-2}, τ = 50 fs, and f_0 = 0 as a function of the distance x to the target surface.

Thus, when only field ionisation is taken into account at distances of 75–150 μm above the target surface, the electron density does not reach the required level. Moreover, with increasing FS pulse duration, the maxima of γ-radiation and three-halves harmonic yields are shifted from the target surface, whereas a decrease in the FS radiation intensity reduces the multiplicity Z_f of field ionisation (Fig. 7a), the probability of which depends exponentially on the laser field intensity [20].

The presence of a sufficiently large electron density above the target surface in the case of a 'long' FS pulse can be explained if we take into consideration the process of collisional ionisation of atoms in plasma by electrons oscillating in the laser field.

Although already at the FS pulse front, all the atoms located in the electromagnetic field of the pulse turn out ionised, the maximum multiplicity Z_f of their ionisation is determined by the relation of the corresponding energy of successive ionisation of an atom and the field intensity at the point of atom location. The collisional ionisation rate of an atom is much lower than the corresponding field ionisation rate; however, with a sufficient FS pulse duration, an increase in the number of free electrons in the absence of recombination leads to an avalanche-like increase in the electron density: $n_e = n_{e0}\exp(\nu_{imp}\tau)$, where n_{e0} is the initial electron density [22] (Fig. 7b).

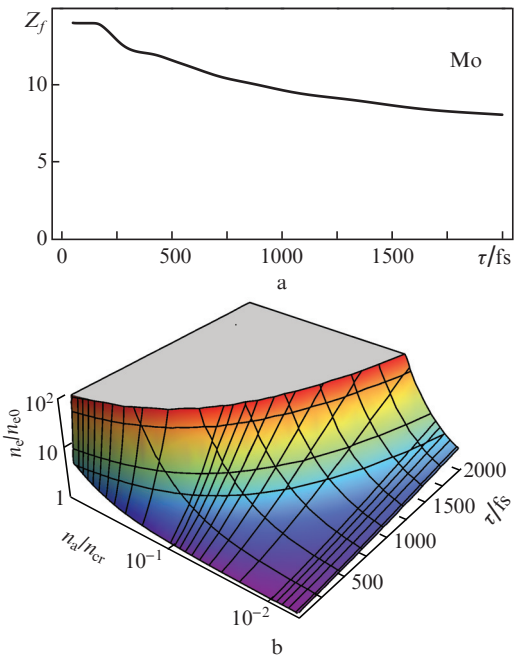

Figure 7. (Colour online) (a) Dependence of the multiplicity of sequential field ionisation of Mo atoms at the FS radiation focus on the pulse duration; (b) ratio of the final electron density n_e formed as a result of collisional ionisation of Mo^{6+} ions to the initial density n_{e0} at the FS radiation focus as a function of the pulse duration τ and atomic density n_a. The integral energy flux density of the FS pulse is $F_0 \approx 1.5 \times 10^5$ J cm^{-2}.

The probability $\nu_{imp}(n_a, \varepsilon_{osc})$ of a single collisional ionisation (per unit time) in plasma with atomic density n_a by a single electron oscillating with a maximum energy ε_{osc} in a laser field is defined as [22, 23]

$$n_a \sum_i \int_{I_i}^{\varepsilon_{osc}} \sqrt{2\varepsilon/m_e}\, \sigma_i^{imp}(\varepsilon) f_\varepsilon(\varepsilon)\, d\varepsilon .$$

We assume that the energy distribution of electrons is given by the delta function, $f_\varepsilon(\varepsilon) = \delta(\varepsilon - \langle\varepsilon\rangle)$, i.e., they collide with atoms at an average kinetic energy equal to the energy of their oscillatory motion in a plane electromagnetic wave: $\langle\varepsilon\rangle = \varepsilon_{osc}/2 = (e^2/(2\pi m_e c^3))I\lambda_0^2$, where e and m_e are the charge and mass of the electron and c is the speed of light in vacuum. At $I\lambda_0^2 = 10^{17}-10^{18}$ (W cm^{-2}) μm^2, the energy $\langle\varepsilon\rangle$ is ~10–100 keV, and the amplitude of electron oscillations in the field is approximately 30–90 nm, which is significantly greater than the average distance between ions in plasma ($n_a^{-1/3}$ = 4 nm at $n_a = 0.01 n_{cr}$). Let us use the Bethe formula [24, 25] for the cross section $\sigma_i^{imp}(\varepsilon)$ of single ionisation of the ith shell of an atom with ionisation energy I_i [26, 27], containing q_i electrons. Then, for $I_i \ll \langle\varepsilon\rangle < m_e c^2$, we obtain

$$\nu_{imp}(n_a, \varepsilon_{osc}) \approx n_a \sum_i \sqrt{\frac{\varepsilon_{osc}}{m_e}}\, q_i 4\pi a_B^2 \left(\frac{\mathrm{Ry}}{I_i}\right)^2 \frac{\ln(\varepsilon_{osc}/(2I_i))}{\varepsilon_{osc}/(2I_i)},$$

where $\mathrm{Ry} = e^2/(2a_B)$, a_B is the Bohr radius, and summation is performed over all filled shells. Figure 8a shows the result of calculating the electron density profile $n_e(x)$ when the FS pulse with a duration $\tau = 600$ fs propagates in plasma with allowance for field and collisional ionisations. The initial atomic density profile was set in the form $n_{a0}(x)/n_{cr} = 1.5\exp(-x/10) + 0.025\exp(-x/150)$ (x in micrometers), which corresponds to the profile obtained in interferometry experiments in the second maximum region.

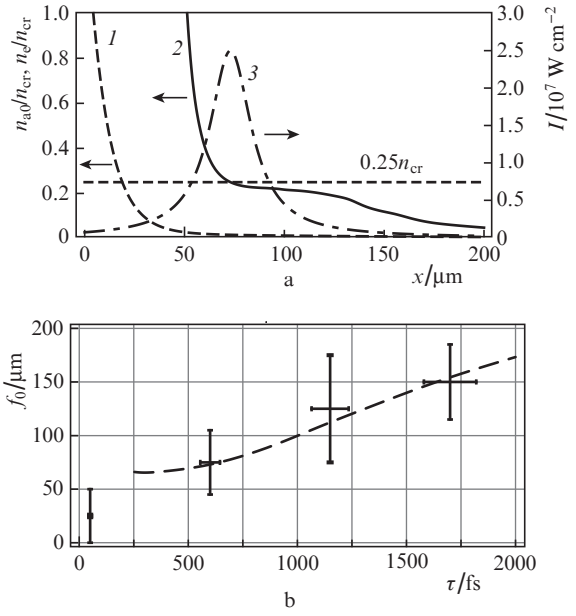

Figure 8. (a) Initial atomic density profile $n_{a0}(x)/n_{cr}$ corresponding to the region of the second maximum (*1*), the calculated electron density profile $n_e/n_{cr} = (n_{a0}/n_{cr})Z_f\exp(\nu_{imp}\tau)$ for the FS pulse duration $\tau = 600$ fs and focusing to point $f_0 = 73$ μm (*2*), dependence of the FS pulse intensity on the distance x to the target surface (*3*); (b) experimental data (vertical bars show the sizes of the region of the second maximum with respect to the focus, horizontal bars show the error in determining the FS pulse duration) and the calculated dependence of the position $x_0 = f_0$ of the second maximum with respect to the focus on the FS laser pulse duration (dashed curve).

The above model does not take into account the processes of multiple ionisation, the existence of excited states of atoms and ions, changes in the ionisation energies I_i of ions [28] compared to neutral atoms, etc. Nevertheless, it allows us to demonstrate a shift of the FS pulse focusing region, in which a second maximum is observed in the direction from the target surface as the FS pulse duration increases.

Our experimental studies have shown that the regions of an increased γ-radiation yield and the excitation of plasma waves approximately coincide. As the duration τ increases, the FS radiation intensity decreases significantly (up to $I \approx 5\times10^{16}$ W cm^{-2} at $\tau \sim 2000$ fs); therefore, the most efficient excitation of plasma waves occurs near the focusing point of FS radiation. In addition, the growth increments of parametric processes leading to the excitation of plasma waves reach a maximum at $n_e \approx n_{cr}/4$. Thus, the second maximum is located at the point x_0 above the target surface, which coincides with the FS pulse focusing point f_0, the electron density at which reaches a threshold value $n_e^{th} = n_{cr}/4$. The dependence $x_0(\tau)$ defined by the equation $n_e^{th} = Z_f(x_0, \tau, x_0, F_0)n_{a0}(x_0)\exp[\nu_{imp}(n_{a0}(x_0), \varepsilon_{osc}(\tau))\tau]$, where $\varepsilon_{osc}(\tau) = \varepsilon_{osc}^0\tau_0/\tau$, $\varepsilon_{osc}^0 \propto I_0\lambda_0^2$ is the oscillatory energy at a minimum duration τ_0 of the FS pulse and $Z_f(x_0, \tau, x_0, F_0)$ is the field ionisation multiplicity at the point x_0 that coincides with the focusing point of the FS pulse of duration τ, is shown in Fig. 8b.

Another effect that occurs as a result of collisional ionisation should be mentioned. Since the probability of field ionisation increases with increasing laser radiation intensity, a radial gradient of the electron density dn_e/dr is formed, so that the density decreases from the laser beam axis to its periphery, which leads to defocusing of the beam [1]. Collisional ionisation, on the contrary, results in the formation of an oppositely directed radial gradient of electron density, which prevents the beam from broadening, in the focal waist region. This is because $\varepsilon_{osc} \gg I_i$ near the focus on the beam axis for most atomic shells, whereas the probability of collisional ionisation appears as

$$\nu_{imp} \propto \frac{\ln(\varepsilon_{osc}/(2I_i))}{\varepsilon_{osc}/(2I_i)}$$

and reaches a maximum at the beam periphery at $\varepsilon_{osc} \sim 2\mathrm{e}I_i$, where e is the Euler number.

Thus, the estimates show that collisional ionisation in the FS pulse field leads to an increase in the electron density to values at which efficient excitation of plasma waves and the generation of the three-halves harmonic of the FS pulse are possible.

5. Numerical simulation

To clarify the mechanism of generation of electrons with energies significantly exceeding the oscillatory ones (up to 2 MeV at $\varepsilon_{osc} \sim 16$ keV for $\tau = 1150$ fs), we performed numerical simulation by the particle-in-cell (PIC) method using the Mandor code [29] in the 2D3V regime. The time step was 0.003 fs, while the spatial step was $\lambda_0/100 = 0.01$ μm. The size of the computational domain was 47×10 μm. We used the following initial parameters: $I = 2.5\times10^{17}$ W cm^{-2}, $\tau = 600$ fs, and a beam diameter (FWHM) of 2.5 μm. The profile shown in Fig. 8a, calculated with allowance for field and collisional ionisation, was taken as the initial electron density profile n_e. In the course of PIC simulation, ionisation was considered frozen.

The simulation has shown that plasma waves with wavenumbers $k_p \approx 0.6\omega_0/c$ are excited in the plasma region with electron densities $n_e = 0.2-0.25n_{cr}$ (Fig. 9a). Let us show that their generation is stipulated by forward stimulated Raman scattering (SRS) [1].

In the case of forward SRS, a laser electromagnetic wave with frequency ω_0 and wave vector $\boldsymbol{k}_p$ is split into Stokes electromagnetic (ω_s, $\boldsymbol{k}_s$) and plasma (ω_p, $\boldsymbol{k}_p$) waves, with the Stokes wave propagating in the same direction as the laser one. The electron density $n_e = 0.21n_{cr}$ corresponds to the plasma frequency $\omega_p = (4\pi e^2 n_e/m_e)^{1/2} = 0.46\omega_0$ and to the wave vector of the laser wave $k_0 = (1-n_e/n_{cr})^{1/2}\omega_0/c = 0.89\omega_0/c$. Based on the dispersion relation $\omega^2 = \omega_p^2 + k^2c^2$ for an electromagnetic wave (ω, $\boldsymbol{k}$) in plasma and the conservation laws $\omega_0 = \omega_s + \omega_p$, $k_0 = k_s + k_p$ [30], we can calculate the frequency $\omega_s = 0.54\omega_0$ and the wave vector $k_s = 0.28\omega_0/c$ of the Stokes wave. Then the wave vector of the plasma wave is $k_p = 0.6\omega_0/c$, which corresponds to the calculation.

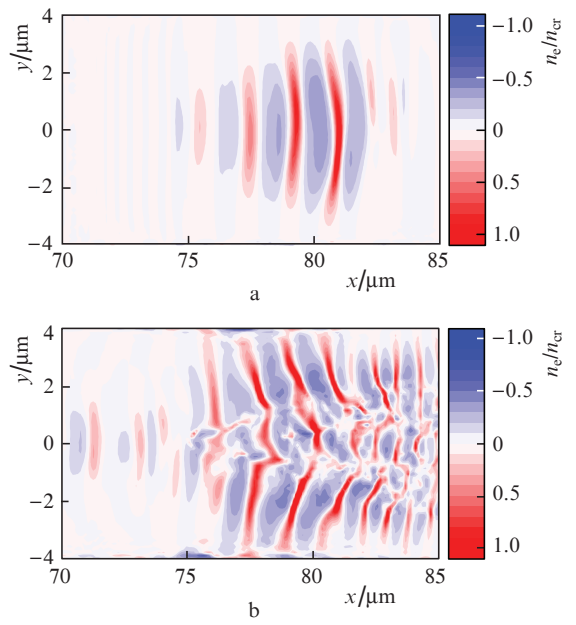

Figure 9. (Colour online) Electron density deviation from the equilibrium one (a) at the time moment of the plasma waves occurrence (t = 245 fs from the simulation start) and (b) at their decay (t = 266 fs) as a function of the distances to the target surface (x) and to the laser beam axis (y).

Thus, a wave of electron density with a phase velocity $v_{ph} = \omega_p/k_p = 0.77c$ is excited in plasma. The generation of high-energy electrons occurs at the time moment of destruction of such a wave (Fig. 9b). The momentum that the electron can aquire is estimated [1] as $\Delta p = eE_{wb}\Delta t$, where $E_{wb} = m_e\omega_p v_{ph}/e \approx 1.4$ TV m^{-1} is the maximum field at the threshold of plasma wave breaking, and $\Delta t = (\pi/k_p)/(c - v_{ph}) \approx 10$ fs is the time that an electron travelling with a velocity close to the speed of light is in the accelerating phase until the sign of the field intensity changes. Then $\Delta p = \pi m_e v_{ph}^2/(c - v_{ph}) \approx 8m_e c$, and the kinetic energy of electron is $\varepsilon = m_e c^2 \times \left(\sqrt{1 + (\Delta p/(m_e c))^2} - 1\right) \approx 3.6$ MeV. The resulting energy estimate within acceptable limits corresponds to the electron spectrum obtained in the numerical experiment (Fig. 10).

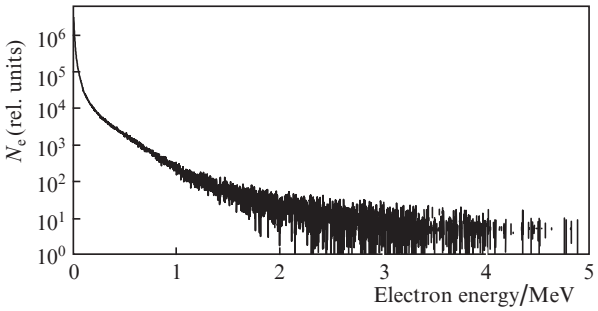

Figure 10. Numerically calculated electron energy spectrum at the time moment t = 275 fs from the beginning of the simulation.

6. Conclusions

We have shown that increasing the main FS pulse duration from 50 to 1700 fs at a constant energy (corresponding to an intensity $I \approx 3\times10^{18}$ W cm^{-2} for a duration of 50 fs) leads to an increase in the yield of bremsstrahlung γ-radiation by more than 10 times with the NS pulse being ahead of the FS pulse by approximately 15–20 ns (the second maximum on the maps of the γ-radiation yield from plasma). The described effect is not observed with an increased (from 10^{-7} to 10^{-9}) ASE level contrast of the FS pulse.

With an increased FS pulse duration in the region of the second maximum, the processes of excitation and decay of plasma waves lead to the generation of fast electrons at $n_e \approx n_{cr}/4$. This is indicated by the coincidence of the FS pulse focusing regions in which a maximum yield of γ-radiation and three-halves harmonic of FS radiation is observed, as well as by the same tendency to shifting these regions from the target surface with an increase in the FS pulse duration. In this case, the required electron density profile is formed as a result of additional ablation under the ASE action and due to collisional ionisation by electrons oscillating in the field of a long FS pulse. Estimates and numerical PIC simulations performed for this profile have shown that electrons can be accelerated as a result of the breaking of plasma waves excited due to SRS up to energies that significantly exceed the oscillatory energy in the FS pulse field. As the FS pulse lengthens, the plasma volume in which plasma waves are excited also increases, which leads to an increase in the number of accelerated electrons and an increase in the γ-radiation yield.

We should note that due to collisional ionisation, the described mechanism of modifying the electron density profile can play a significant role in the interaction of long (more than 250 fs) laser pulses with matter. In particular, this may be significant in experiments using high-power Nd : glass laser systems, such as Phelix [31] and Vulcan [32], which generate subpicosecond pulses.

Acknowledgements. This study was supported by the Russian Foundation for Basic Research (Research Project Nos 19-02-00104 and 19-32-60069) and performed using the equipment of the shared research facilities of HPC computing resources at Lomonosov Moscow State University.

References

1. Gibbon P. *Short Pulse Laser Interactions with Matter* (Imperial College Press, 2005).
2. Umstadter D. *J. Phys. D: Appl. Phys.*, **36**, R151 (2003).
3. Mourou G.A., Tajima T., Bulanov S.V. *Rev. Mod. Phys.*, **78**, 309 (2006).
4. Wagner F., Bedacht S., Ortner A., Roth M., Tauschwitz A., Zielbauer B., Bagnoud V. *Opt. Express*, **22**, 29505 (2014).
5. Mandal T., Arora V., Rao B.S., Moorti A., Upadhyay A., Chakera J.A. *Phys. Plasmas*, **26**, 043105 (2019).
6. Borm B., Khaghani D., Neumayer P. *Phys. Plasmas*, **26**, 023109 (2019).
7. Rao B.S., Arora V., Naik P.A., Gupta P.D. *Phys. Plasmas*, **19**, 113118 (2012).
8. Ivanov K.A., Shulyapov S.A., Ksenofontov P.A., Tsymbalov I.N., Volkov R.V., Savel'ev A.B., Brantov A.V., Bychenkov V.Yu., Turinge A.A., Lapik A.M., Rusakov A.V., Djilkibaev R.M., Nedorezov V.G. *Phys. Plasmas*, **21**, 093110 (2014).
9. Chen H., Shepherd R., Chung H.K., Kemp A., Hansen S.B., Wilks S.C., Ping Y., Widmann K., Fournier K.B., Dyer G., Faenov A., Pikuz T., Beiersdorfer P. *Phys. Rev. E*, **76**, 056402 (2007).
10. Shulyapov S.A., Ivanov K.A., Tsymbalov I.N., Krestovskih D.A., Savel'ev A.B., Ksenofontov P.A., Brantov A.V., Bychenkov V.Yu. *J. Phys. Conf. Ser.*, **653**, 012007 (2015).
11. Ivanov K.A., Tsymbalov I.N., Shulyapov S.A., Krestovskih D.A., Brantov A.V., Bychenkov V.Yu., Volkov R.V., Savel'ev A.B. *Phys. Plasmas*, **24**, 063109 (2017).

12. Tsymbalov I., Gorlova D., Shulyapov S., Prokudin V., Zavorotny A., Ivanov K., Volkov R., Bychenkov V., Nedorezov V., Paskhalov A., Eremin N., Savel'ev A. *Plasma Phys. Control. Fusion*, **61**, 075016 (2019).
13. Kalashnikov M.P., Osvay K., Priebe G., Ehrentraut L., Steinke S. Sandner W. *AIP Conf. Proc*., **1462**, 108 (2012).
14. Ivanov K.A., Shulyapov S.A., Rusakov A.V., Turinge A.A., Brantov A.V., Savel'ev A.B., Djilkibaev R.M., Nedorezov V.G., Uryupina D.S., Volkov R.V., Bychenkov V.Yu. *Phys. Part. Nucl. Lett*., **11**, 54 (2014).
15. Krestovskikh D.A., Ivanov K.A., Tsymbalov I.N., Shulyapov S.A., Bukin V.V., Volkov R.V., Rupasov A.A., Savel'yev A.B. *Quantum Electron*., **47**, 42 (2017) [*Kvantovaya Elektron*., **47**, 42 (2017)].
16. Le Blanc S.P., Sauerbrey R., Rae S.C., Burnett K. *J. Opt. Soc. Am. B*, **10**, 1801 (1993).
17. Veisz L., Theobald W., Feurer T., Schwoerer H., Uschmann I., Renner O., Sauerbrey R. *Phys. Plasmas*, **11**, 3311 (2004).
18. Tarasevitch A., Dietrich C., Blome C., Sokolowski-Tinten K., Von der Linde D. *Phys. Rev. E*, **68**, 026410 (2003).
19. Burnett N.H., Corkum P.B. *J. Opt. Soc. Am. B*, **6**, 1195 (1989).
20. Landau L.D., Lifshits E.M. *Course of Theoretical Physics. Vol. 3. Quantum Mechanics: Non-Relativistic Theory* (Oxford, Waltham, Massachusetts: Butterworth-Heinemann, 1981; Moscow: Fizmatlit, 2004).
21. Keldysh L.V. *Zh. Eksp. Teor. Fiz*., **47**, 1945 (1965).
22. Sobelman I.I., Vainshtein L.A., Yukov E.A. *Excitation of Atoms and Broadening of Spectral Lines* (Berlin, Heidelberg: Springer-Verlag, 1981; Moscow: Nauka, 1979).
23. Ditmire T., Donnelly T., Rubenchik A.M., Falcone R.W., Perry M.D. *Phys. Rev. A*, **53**, 3379 (1996).
24. Bethe H. *Ann. Phys*., **397**, 325 (1930).
25. Kim Y.K., Rudd M.E. *Phys. Rev. A*, **50**, 3954 (1994).
26. Blokhin M.A., Shveitser I.G. *Rentgenospektral'nyi spravochnik* (X-ray Spectroscopy Handbook) (Moscow: Nauka, 1982).
27. Kramida A., Ralchenko Y., Reader J. and NIST ASD Team (2019). NIST Atomic Spectra Database (ver. 5.7.1) (National Institute of Standards and Technology, Gaithersburg, MD).
28. Carlson T.A., Nestor C.W. Jr, Wasserman N., McDowell J.D. *At. Data Nucl. Data Tables*, **2**, 63 (1970).
29. Romanov D.V., Bychenkov V.Yu., Rozmus W., Capjack C.E., Fedosejevs R. *Phys. Rev. Lett*., **93**, 215004 (2004).
30. Kruer W.L. *The Physics of Laser Plasma Interactions* (Redwood City: Addison-Wesley, 1988).
31. Rosmej O.N., Andreev N.E., Zaehter S., Zahn N., Christ P., Borm B., Radon T., Sokolov A., Pugachev L.P., Khaghani D., Horst F., Borisenko N.G., Sklizkov G., Pimenov V.G. *New J. Phys*., **21**, 043044 (2019).
32. Danson C.N., Brummitt P.A., Clarke R.J., Collier J.L., Fell B., Frackiewicz A.J., Hawkes S., Hernandez-Gomez C., Holligan P., Hutchinson M.H.R., Kidd A., Lester W.J., Musgrave I.O., Neely D., Neville D.R., Norreys P.A., Pepler D.A., Reason C.J., Shaikh W., Winstone T.B., Wyatt R.W.W., Wyborn B.E. *Laser Part. Beams*, **23**, 87 (2005).